GEOLOGY

Rare earth element mobility in and around carbonatites controlled by sodium, potassium, and silica

Michael Anenburg[1,2]*, John A. Mavrogenes[1], Corinne Frigo[1], Frances Wall[2]

Carbonatites and associated rocks are the main source of rare earth elements (REEs), metals essential to modern technologies. REE mineralization occurs in hydrothermal assemblages within or near carbonatites, suggesting aqueous transport of REE. We conducted experiments from 1200°C and 1.5 GPa to 200°C and 0.2 GPa using light (La) and heavy (Dy) REE, crystallizing fluorapatite intergrown with calcite through dolomite to ankerite. All experiments contained solutions with anions previously thought to mobilize REE (chloride, fluoride, and carbonate), but REEs were extensively soluble only when alkalis were present. Dysprosium was more soluble than lanthanum when alkali complexed. Addition of silica either traps REE in early crystallizing apatite or negates solubility increases by immobilizing alkalis in silicates. Anionic species such as halogens and carbonates are not sufficient for REE mobility. Additional complexing with alkalis is required for substantial REE transport in and around carbonatites as a precursor for economic grade-mineralization.

INTRODUCTION

Demand for rare earth elements (REEs; Y and the lanthanides La-Lu) will increase rapidly as the world decarbonizes (*1*–*3*). Additional supplies of REE, especially Nd, Pr, and smaller amounts of Dy, are required to manufacture high-strength permanent magnets for direct drive motors in wind turbines, electric vehicles, and other low-carbon technologies. The REE also have uses as enablers of many technologies, from catalysts, phosphors, and ceramics to antiforgery, lasers, and medicine (*4*–*7*).

Primitive and unfractionated REE abundances in natural rocks follow two trends: decrease of absolute abundance with increasing atomic number (e.g., La and Ce and more abundant than Yb and Lu) and the Oddo-Harkins rule, which states that REEs with even atomic numbers are more abundant than their neighboring odd-numbered elements (e.g., Ce is more abundant than La and Pr). The geochemical behavior of REE is controlled by the "lanthanide contraction"—the decreasing REE^{3+} cation size from La to Lu, which often results in gentle fractionation of light (La-Sm) away from heavy (Eu-Lu and Y) REE, but almost never the isolation of individual elements (Eu^{2+} and Ce^{4+} excepted) (*5*, *6*).

Carbonatites are carbonate-dominated rocks of igneous origin. These rare rocks and their altered and weathered derivatives provide most of the world's REE (*2*, *4*, *7*, *8*). The lanthanide contraction coupled with the uneven absolute abundances of the REE contrives to exclude the possibility of a "Nd deposit," for example. Any deposit mined for Nd will always contain more Ce than Nd and often more La as well (*2*, *7*). This presents a challenge for geologists, who now must find not just deposits rich in REE, but deposits that have proportions closest to industry needs. Demand for electric vehicle motors is forecast to increase in the coming decades. Therefore, deposits should have as much Nd and Pr as possible compared to La and Ce, with a sprinkling of Dy to make the perfect REE combination for magnets. They should also have a favorable mineralogy for separation of ore from gangue and should be reasonably low in the radioactive elements Th and U (*4*, *7*). Our need for responsible mining and greater resilience to global supply-chain disruption necessitates diversification of mining localities (*1*, *6*, *9*).

It has long been established that REE deposits are associated with late hydrothermal activity in and around carbonatites due to ubiquitous sub-solidus alteration (*4*, *8*, *10*–*13*). Aureoles of REE-rich sodic or potassic metasomatic alteration, or fenites, are common around carbonatites and can extend up to 4 km from the main intrusions (*10*, *13*). No unified model explains all features of carbonatite-associated REE deposits, strongly impairing exploration required to secure future supply. Most REE mobility studies focused on anionic complexing ligands and overlooked the role of dissolved alkali cations. Here, we isolate the effect of Na^+ and K^+ from anions on REE solubility. This study provides previously unknown experimental constraints on the late-stage evolution of carbonatite magmas, REE solubility in aqueous carbonate-rich fluids, and the likely compositions of REE minerals that form during this process.

Capsule-scale carbonatite–REE deposits

In an effort to qualitatively establish chemical factors that favor REE transport, we performed a series of cooling experiments of REE-bearing carbonatites of variable composition (Table 1). To simplify analysis, we added only one light REE (LREE; La) and one heavy REE (HREE; Dy) to each experiment to establish what controls heavy versus LREE mobility. We performed four piston-cylinder experiments in which we slowly cooled and decompressed synthetic carbonatite compositions analogous to natural carbonatite liquids. The first run consisted of a Ca-Mg-Fe-P-F–carbonatite composition, together with $Ca(Cl,Br)_2$ solution in a silver capsule (run CbX; Table 1). Subsequent experiments contained additional SiO_2 (run CbSi), Na_2CO_3 (run CbNa), or K_2CO_3 (run CbK) in nickel capsules (Table 1). Experiments started at 1050°C and 2.5 GPa (run CbX) or 1200°C and 1.5 GPa (runs CbSi, CbNa, and CbK), gradually decompressed and cooled on a linear path to 200°C and 0.2 GPa after 4 days (all experiments), and finished by quenching from 200°C to room temperature (see fig. S1).

RESULTS

All experimental assemblages were initially molten and crystallized from the capsule walls inward with magmatic phases at the extremities

[1]Research School of Earth Sciences, Australian National University, Canberra ACT 2600, Australia. [2]Camborne School of Mines, University of Exeter, Penryn, TR10 9FE, UK. *Corresponding author. Email: michael.anenburg@anu.edu.au

Table 1. Starting material compositions for piston cylinder experiments.

	CbX	CbSi	CbNa	CbK
$CaCO_3$ (%)	65.0	53.2	56.0	54.2
$MgCO_3$ (%)	15.0	12.3	12.9	12.5
$FePO_4$ (%)	14.0	11.5	12.1	11.7
MgF_2 (%)	3.5	2.9	3.0	2.9
$MgCl_2$ (%)	1.3	1.1	1.1	1.1
Dy_2O_3 (%)	0.6	0.5	0.5	0.5
La_2O_3 (%)	0.6	0.5	0.5	0.5
SiO_2 (%)	0	18.1	0	0
Na_2CO_3 (%)	0	0	13.9	0
K_2CO_3 (%)	0	0	0	16.6
Total added (mg)	196.4	198.3	188.2	202.2
1 M $CaBr_2$ (mg)	16.6	14.9	10.5	11.9
CaO	34.02	28.12	30.00	28.99
MgO	9.21	7.60	8.14	7.86
Fe_2O_3	6.83	5.64	6.04	5.84
P_2O_5	6.07	5.02	5.37	5.19
Na_2O	0	0	7.70	0
K_2O	0	0	0	10.69
SiO_2	0	16.88	0	0
La_2O_3	0.55	0.46	0.49	0.47
Dy_2O_3	0.55	0.46	0.49	0.47
CO_2	33.57	27.72	35.16	33.67
H_2O	6.24	5.59	4.23	4.45
F	1.97	1.63	1.74	1.68
Cl	0.89	0.74	0.79	0.76
Br	1.25	1.12	0.84	0.89
—F, Cl, and Br═O	−1.15	−0.96	−0.99	−0.97

of each capsule and hydrothermal phases toward the capsule center (Fig. 1). A magmatic-hydrothermal volatile phase created a hydrothermal cavity, in which dissolved species precipitated during quench. The higher initial pressure of run CbX caused early crystallization of elongate aragonite, which then transformed to calcite during decompression (Fig. 1). As a result, the high-temperature and low-temperature regions are not separated in this run but are still distinguishable.

The magmatic assemblage is uniform across all experiments and consists of Mg-bearing calcite followed by dolomite with increasing ankeritic component, co-crystallized with carbonate-bearing, REE-poor [<1 weight % (wt %)] fluorapatite (e.g., Figs. 1, 2A, and 3, and the Supplementary Materials). Run CbSi contains forsteritic olivine and augitic clinopyroxene in addition to the carbonates. Furthermore, fluorapatite cores of run CbSi contain elevated REE contents (up to ~1.5 wt % La_2O_3 and 2.5 wt % Dy_2O_3).

The hydrothermal (low-temperature) assemblages of all runs consist of zoned magnesite with increasing Fe ± Ni (siderite ± gaspéite) contents that line the cavities, in contact with dolomite-ankerite (Fig. 2, B and C). The outermost rims of the low-temperature carbonates contain Dy (Fig. 2C and Table 2). Hydrothermal fluorapatite and carbonates within the cavities have high-REE rims (Fig. 2, B to D), with variable La/Dy (Fig. 3).

All other phase assemblages vary markedly among runs. Run CbX contains fluorite, sellaite, hematite, bastnäsite, and highly soluble $Ca(Cl,Br)_2$. Fluorite contains occasional growth zones with elevated Dy contents (Table 2). Bastnäsite occurs mainly as elongate crystals with La-rich cores and Dy-rich rims (Fig. 2D).

Run CbSi differs from CbX by the lack of sellaite and hematite and much higher capsule-derived Ni contents in the hydrothermal carbonates, resulting from the incorporation of Mg and Fe into early-crystallizing olivine and clinopyroxene. REE-rich rims on fluorapatite are more abundant than in run CbX and contain overgrowths of britholite-rich fluorapatite. Bastnäsite of run CbSi is modally less abundant and primarily contains La without Dy-rich rims, compared to run CbX (Fig. 2E and Table 2). Two types of REE phosphates occur inside the cavity of run CbSi, with one containing La > Dy and the other Dy > La (qualitatively identified as "monazite" and "xenotime," respectively). However, as their porous nature, low analytical totals (~92%), and small grain sizes (<20 μm) preclude infrared analysis, it is uncertain whether they are well-crystallized anhydrous monazite or xenotime or hydrated equivalents such as rhabdophane or churchite ($LaPO_4{\cdot}nH_2O$ and $DyPO_4{\cdot}nH_2O$, respectively).

Run CbNa contains a variety of Na-rich, low-temperature phases, most of which are highly soluble and very rare in nature. Lining the cavity wall are the fluorides neighborite and cryolite, the phosphate moraskoite, and the carbonates eitelite and rouvilleite. The cavity interior contains nahcolite and bonshtedtite-bradleyite solid solution (Fig. 2F). Most of these nominally REE-free phases contain some La and Dy (Table 2). A burbankite-group mineral occurs both lining the cavity wall and inside the cavity itself. It contains La-rich cores of similar stoichiometry to rémondite and Dy-rich rims. The rims have a total of eight cations per formula unit, of which six are Na (Fig. 2, F and G). Burbankite-group minerals contain only six cations per formula unit, so these rims may not belong to the burbankite group per se, but on the basis of their related chemistry and continuous growth around rémondite, we tentatively name them "natroburbankite." The greater Na contents of natroburbankite indicate higher solubility in the fluid compared to stoichiometric burbankite and therefore greater Dy solubility relative to La in this system. The cavity of run CbNa contains a Na-REE–carbonate-halide phase that occurs as irregular grains or as elongate needles with irregular internal zoning (Fig. 2G). This phase appears to be intergrown with nahcolite and occasionally appears around fluid inclusions or bubbles in the epoxy resin exposed during polishing (Fig. 1). This morphology indicates crystallization during quench from 200°C or subsequently during drying at 110°C before impregnation with epoxy resin. The general characteristics of the cavity fillings in run CbNa remarkably resemble inclusions containing carbonatite-derived fluid inclusions (*14*–*16*).

Run CbK contains fewer phases, with only minor elpasolite and parascandolaite lining the cavity walls (Fig. 1). The cavity interior contains abundant kalicinite and a K-REE–carbonate-halide phase that formed on quench, similar to the REE-quench phase from run CbNa (Fig. 2H and Table 2). It is differentiated by its spherical aggregate rather than acicular habit and by its high Fe and low F contents.

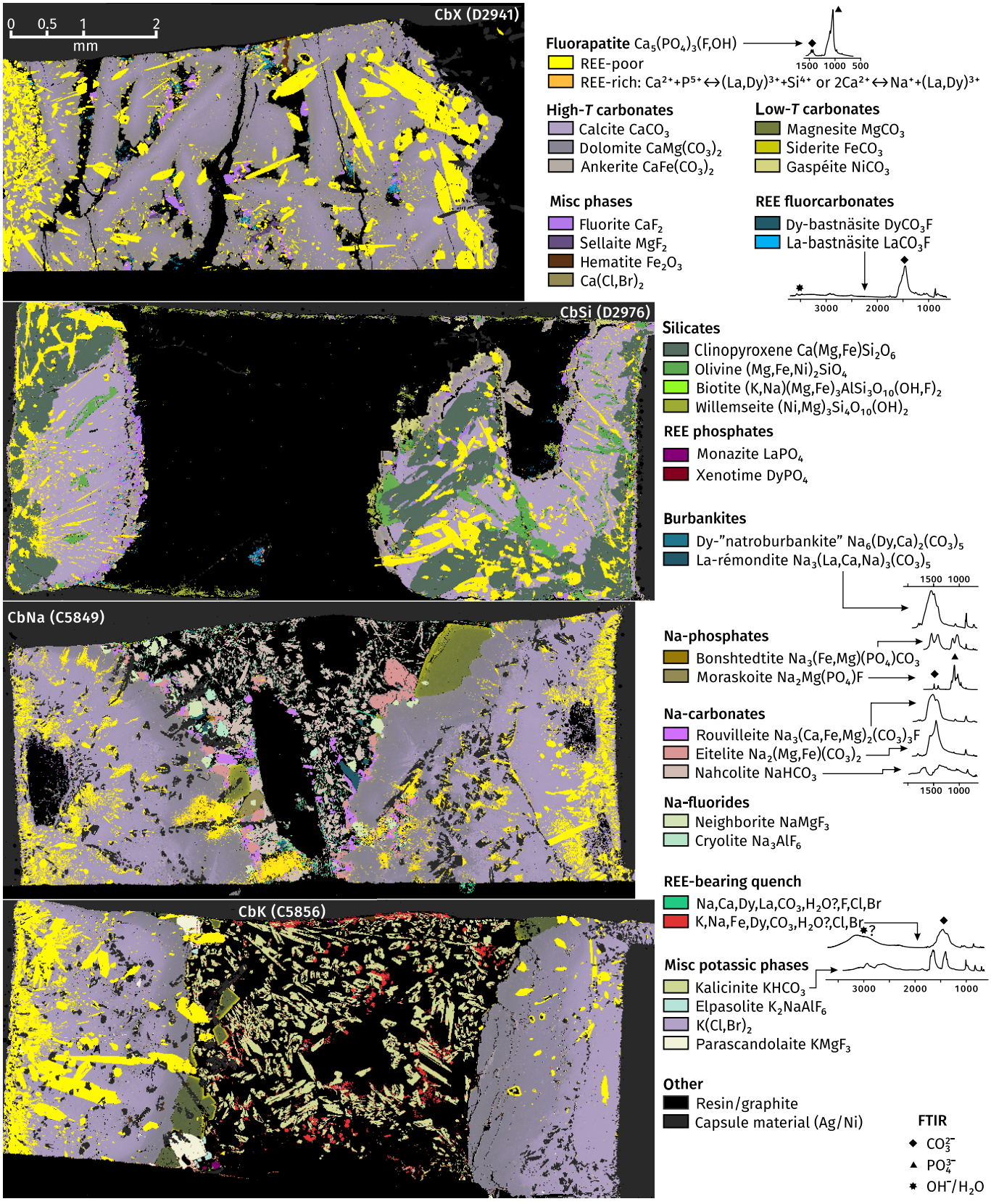

Fig. 1. QEMSCAN mineral identification maps of the experimental runs. Fourier transform infrared (FTIR)–attenuated total reflectance spectra added for selected phases. Maps containing single minerals are available in figs. S2 to S5.

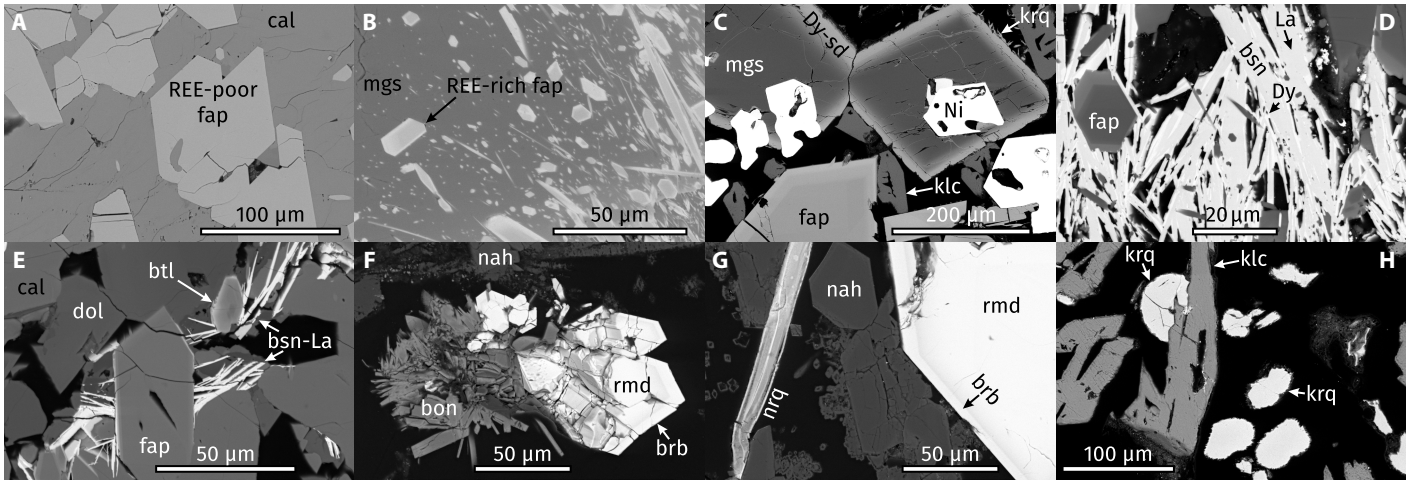

Fig. 2. Backscattered electron images of run products. CbX: (**D**); CbSi: (**E**); CbNa: (**A**), (**B**), (**F**), and (**G**); CbK: (**C**) and (**H**). See text for discussion. Abbreviations: bon, bonshtedtite; brb, natroburbankite; bsn, bastnäsite; btl, britholite; cal, calcite; dol, dolomite; fap, fluorapatite; klc, kalicinite; (k/n)rq, K/Na–REE-quench; mgs, magnesite; nah,nahcolite; rmd, rémondite; sd, siderite.

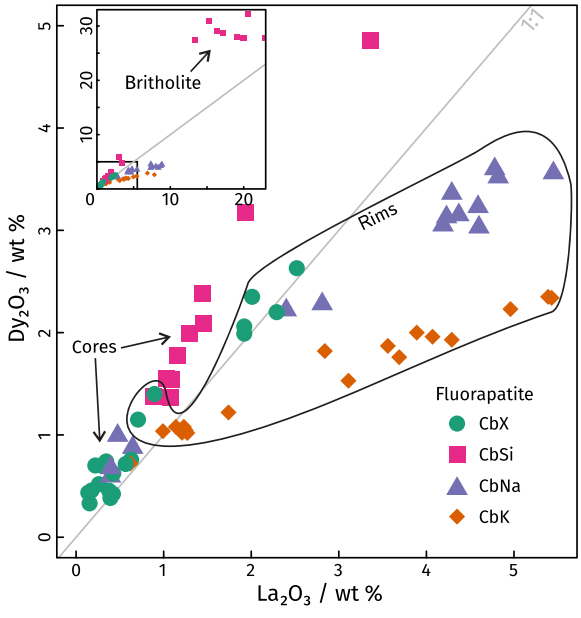

Fig. 3. REE composition of fluorapatite from the experimental runs. The main figure is an enlargement of the small box in the inset. REE-rich points in the inset are britholite.

DISCUSSION

Textural and geochemical trends in run products

During our experiments, magmatic phases crystallized from the capsule walls (left and right of Fig. 1), leaving a hydrous melt and subsequently a hydrothermal fluid trapped in the center. Thus, growth toward the central cavities establishes a fractionation trend. Natural carbonatite compositions often grade from calcite carbonatite to ferroan dolomite/ankerite carbonatite. A good rule of thumb for REE exploration is to look at ferroan dark brown carbonatites formed by oxidation of the ferrous component of late-stage carbonate minerals (*17*). Our experiments mimic the most commonly observed intrusive sequence of rock-forming minerals in carbonatites. The igneous portions contain calcite and dolomite, followed by ankerite, consistent with known carbonatite petrology (*13*, *18*–*21*). Evolution of magnesite or ankerite to siderite is likewise described from natural rocks (*18*, *22*, *23*). Our results show that REEs behave incompatibly throughout igneous differentiation of carbonatites. The REE concentrations increase in the melt as crystallization proceeds and REE minerals such as bastnäsite, monazite, and burbankite precipitate late, in the hydrothermal portion of the capsules.

During carbonatite igneous differentiation, REEs are thought to be fractionated by incorporation into apatite and, to a lesser extent, oxides such as pyrochlore (*13*). Early crystallization of these minerals removes REE from the melt and prevents REE mineralization via late-stage hydrothermal activity (*5*, *24*). Fluorapatite can accommodate REE via two substitution vectors: $Ca^{2+} + P^{5+} \rightarrow REE^{3+} + Si^{4+}$ (the "britholite" component), or $2Ca^{2+} \rightarrow REE^{3+} + Na^{+}$. Both occur in our fluorapatite, either by addition of Si (run CbSi) or Na (run CbNa) or by concentrating Si and Na impurities in nominally Si- or Na-free runs.

The REE enrichment degree of early crystallizing fluorapatite in runs CbX, CbNa, and CbK is not sufficient to fractionate the REE, leading to substantial REE concentrations in the hydrothermal cavity. In contrast, REEs are moderately compatible in fluorapatite in run CbSi (Fig. 3). Fluorapatite is experimentally known to incorporate non-trace REE when SiO_2 activity is high (*25*, *26*), but this is rarely attained in carbonatites owing to buffering of SiO_2 activity to low values by silicate crystallization. In our case, buffering is achieved by the thermodynamic equilibrium: $CaMg(CO_3)_{2(l)} + SiO_2 \leftrightarrow CaMgSi_2O_{6(s)} + CO_{2(g)}$. This reaction releases CO_2, as seen in our experiments by the large cavity in the Si-bearing run CbSi (Fig. 1). At low temperatures, when coexisting dolomite and quartz are stable and the buffering reaction stops, high Dy/La britholite rims formed on fluorapatite (Figs. 2E and 3), consistent with observations from natural carbonatites (*26*–*29*). At this high silica activity stage, La-bearing, Dy-free, bastnäsite and monazite co-crystallized with britholite (*30*). Hydrothermal monazite most likely formed because Ca was sequestered into early-crystallizing clinopyroxene,

Table 2. REE contents of experimental phases. nd, not detected.

	La (wt % ± 1 SD)	Dy (wt % ± 1 SD)
La-bastnäsite	58.1 ± 0.6	3.6 ± 0.4
Dy-bastnäsite	21 ± 4	49 ± 2
Bonshtedtite	0.16 ± 0.05	1.9 ± 0.6
"Natroburbankite"	7.1 ± 0.5	23.6 ± 0.4
Rémondite	34 ± 2	1.6 ± 1.1
Rouvilleite	0.14 ± 0.12	1.2 ± 0.3
Neighborite	0.3 ± 0.2	0.66 ± 0.08
Nahcolite	nd	0.3 ± 0.2
Monazite*	≤55	≤4
Xenotime*	≤25	≤32
K–REE-quench	0.80 ± 0.08	7.5 ± 0.3
Na–REE-quench	2.46 ± 0.06	15.2 ± 0.6
Low-*T* carbonate†	≤0.46	≤1.88
Fluorite†	≤1.2	≤3.5

*Fine-scale intergrowths and porosity only allow for a maximum value.
†Values are given for the REE-richest zones in zoned minerals.

preventing crystallization of low-temperature fluorapatite and leaving behind excess P_2O_5.

Even the highest silica activities accessible in carbonatites cannot lead to complete REE sequestration in high-temperature early fluorapatite. Nonetheless, the moderate REE compatibility in early fluorapatite prevents strong late-stage REE concentration. Therefore, hydrothermal REE-rich phases (monazite and bastnäsite) are modally negligible and when generalized to natural systems are unlikely to form an economic deposit in a Si-rich carbonatite.

Alkali-bearing runs (CbNa and CbK) have similar high-temperature assemblages to the two alkali-free runs, in which the REE behave incompatibly. However, instead of being deposited in the bastnäsite and monazite, they are hosted by a variety of more soluble phases. In run CbNa, REE occur in Na-rich burbankite-group phases. Natural burbankite is a rare and ephemeral mineral, often pseudomorphed by fine-grained assemblages of REE fluorcarbonates, monazite, baryte, strontianite, and rock-forming carbonates (*6*, *27*, *29*–*35*), and occasionally described in fluid inclusions (*15*, *22*, *36*). Our experiments also contain extensive REE hosted in the Na-carbonates bonshtedtite and rouvilleite (table S1). These sodic carbonates are extremely rare in nature, either because they simply do not form or because of their instability during alteration. Nonetheless, they have been reported from similar geological environments such as agpaitic peralkaline rocks, phoscorites, and fenites (*14*, *37*, *38*). In either case, their rarity is a sign of their high solubility and therefore high REE solubility in these systems. These phases were preserved in our experiments due to the closed-system nature in which fluids were confined and slow gradual cooling formation of large crystals. Last, abundant REE remained in solution to 200°C evident by the abundant Na–REE-quench phases. HREE are more soluble than LREE as most La was sequestered in rémondite cores, whereas Dy mostly occurs in later natroburbankite rims and in the quench phase. The overwhelming partitioning of Dy to the fluid and its subsequent deposition allows us to estimate the Dy concentration of the fluid during quench. Taking the Dy contents of the fluid as the Dy contents of the quench phase multiplied by the red to black pixel ratio of map CbK in Fig. 3, the fluid Dy contents were ~75,000 parts per million (ppm) × (4269/109,574) = ~3000 ppm. This solubility is orders of magnitude greater than solubilities of Dy and other HREE previously reported for alkali-free solutions in comparable conditions (*39*–*42*). Even more remarkable, our experiments are fluorapatite saturated, a condition that strongly reduces REE solubility relative to P_2O_5-free solutions (*43*), potentially down to the parts per billion range (*41*). Estimating REE solubility in run CbNa is not as straightforward due to the irregular nature of the REE-quench phase and strong partitioning of La and Dy to REE-phases which were solid during quench. However, since both La and Dy behave similarly during the high-temperature igneous stage in runs CbK and CbNa, we qualitatively estimate that in run CbNa, Dy solubilities were marginally lower, with the addition of significant La contents to the hydrothermal fluid (which in run CbK were sequestered in insoluble monazite).

Complexing ligands and fractionation of HREE from LREE

A long-standing mystery is the identity of the ligands that allow REE mobilization in hydrothermal fluids. Although REE are generally considered immobile in most natural systems, the occurrence of REE-rich minerals of unmistakably hydrothermal genesis attests to their mobility (*8*). In addition, P and F are considered to immobilize REE in hydrothermal systems (*39*–*41*, *43*–*45*). However, many carbonatite-associated hydrothermal veins contain P- and F-bearing minerals such as fluorapatite, monazite, xenotime, and REE fluorcarbonates (*39*, *41*), indicating that REE, P, and F were enigmatically transported together. Various anions have been considered as the complexing ligands, and their relative stabilities under varying pH-temperature conditions have been incorporated into thermodynamic models to explain these observations from nature (*5*, *39*, *46*). Fluids containing Cl^-, F^-, CO_3^{2-}, SO_4^{2-}, and any combination thereof have been invoked to explain hydrothermal REE mineralization (*10*, *14*, *20*, *28*, *41*, *47*–*53*). However, these inferences, based on the occurrence of anions in various phases, fluid inclusions within REE mineralized zones, experiments, and thermodynamic modeling, do not satisfactorily explain differential LREE and HREE mobilization. No specific anion has yet to be singled out as the principal REE-complexing anion in natural systems. Our experimental runs CbX and CbSi show that none of these anions (nor Br^-) are important complexing ligands on their own. Had these anions been sufficient for retaining large amounts of dissolved REE, then REE-bearing quench phases should have been formed. That did not occur, and the only quench phases observed in runs CbX and CbSi were $CaCl_2$ and $CaBr_2$. In these alkali-free runs, REE are hosted in bastnäsite and monazite, which were already solid upon quench. Monazite, bastnäsite, and other calcic REE fluorcarbonates are typically insoluble in carbonatite-associated hydrothermal systems (*41*, *54*). They are rarely altered and instead often form as the insoluble residue after other more soluble REE phases such as burbankite destabilize (*31*, *33*). Therefore, REE(±Ca) fluorcarbonates and monazite prevent REE transport by alkali-free carbonatite–derived hydrothermal fluids. If these minerals formed throughout an entire carbonatite intrusion, then the REE would be dispersed over a large volume, leading to greatly reduced economic potential of the system.

Massive solubility increases were observed in the alkali-bearing runs CbNa and CbK, evident by the REE-quench phases. These runs contained abundant carbonate, which remained dissolved to low temperatures because the alkalis were added as soluble Na_2CO_3 and K_2CO_3. In contrast, initially introduced carbonate in runs CbX and CbSi was mostly locked up in the relatively insoluble calcite and dolomite. Therefore, it may be suggested that REE-carbonate complexes are the solubility drivers in runs CbNa and CbK. However, CO_2 was generated in run CbSi during silicate crystallization, providing a carbonate source. Yet, REE solubility in run CbSi does not reach the levels observed in runs CbNa and CbK. This excludes carbonate as the principal complexing ligand, indicating that Na-REE and K-REE complexes are the dominant complexes stable in hydrothermal fluids that allow REE mobilization. The relative fractionation of La from Dy in runs CbNa versus CbK also indicates direct involvement of the alkalis in REE complexing, as all other potential ligands were unchanged in the two alkali-bearing runs. The identities of the anions that charge balance these cationic complexes are unknown and could be fluoride, chloride, carbonate, or a combination thereof. In either case, these anions are abundant in most, if not all, carbonatites. A previous study at 2.6 GPa and 600° to 800°C showed that while NaCl- and NaF-bearing fluids primarily solubilize LREE from $REE_2Si_2O_7$, Na_2CO_3-bearing fluids led to similar dissolution of all REE (*46*). In our run CbNa, however, Dy (an HREE) is an order of magnitude more soluble than La (a LREE); thus, it is highly plausible that the main driver for REE solubility in our experiment is Na_2CO_3 (as it is a carbonatitic system), with the other available ligands amplifying the alkali carbonate effect.

Higher HREE/LREE ratios (including higher Nd) occur when REE are hydrothermally mobilized, for instance, by reworking earlier carbonatite as at Songwe Hill, Malawi (*55*), Ruvubu, Burundi (*56*), Fen, Norway (*57*, *58*), in and around a dyke swarm at Lofdal, Namibia (*59*), at Juquiá, Brazil (*60*), or at shallow depths at Saint-Honoré, Canada (*23*). The relative incompatibility and solubility of LREE versus HREE are strongly controlled by Si, Na, and K. High silica leads to higher HREE/LREE in fluorapatite, which in run CbSi caused a lack of Dy-bastnäsite as Dy was partitioned into fluorapatite and britholite. In contrast, alkalis led to lower HREE/LREE in fluorapatite (Fig. 3), which in runs CbNa and CbK contributed to the exceptional concentration of Dy in the late-stage fluid. Alkalis also contribute to the LREE-HREE fractionation in the hydrothermal fluid. In run CbNa, La is preferentially hosted in rémondite, whereas Dy is primarily hosted in the quench phase. Therefore, although both are soluble, the HREE are more soluble than the LREE. The LREE-HREE decoupling in run CbK is even more extreme in this regard, since La is hosted by the relatively insoluble monazite, whereas Dy is completely partitioned into the K–REE-quench phase (Table 2). Similar HREE/LREE fractionating in potassic fluid was previously observed in higher-temperature solubility studies (*40*). In contrast, LREE-chloride complexes are more stable than HREE-chloride complexes (*5*, *39*, *47*). However, as our alkali-bearing runs show the opposite (i.e., higher HREE solubility), chloride complexing cannot be the solubility-determining factor.

Controls on REE transport

It has long been recognized that the key stage of REE enrichment takes place in transitional environments, after magma fractionation and as REE-bearing fluids exsolve from the carbonatitic melt due to cooling and decompression (*6*, *61*). Carbonatite-related REE deposits mostly form at shallow depths in the upper crust (<5 km), most probably in intrusions that did not erupt (*13*, *16*, *19*), allowing a carbonatite-derived hydrothermal fluid to circulate in and around the carbonatite (*55*, *56*, *62*). The greater solubility of alkali-dominated REE complexes allows their long-distance mobility. These REE-rich fluids will move along structural conduits and concentrate in traps (*19*, *56*, *62*, *63*). If these traps are still within the carbonatites, then crystallization of sodic phases will occur similar to our run CbNa. Burbankite-group minerals are probably the main REE hosts in these cases (*27*, *61*, *64*). Once the hydrothermal activity evolves from carbonatitic composition (e.g., by mixing with groundwater), the sodic minerals destabilize and are replaced by bastnäsite, ancylite, monazite, and other calcic REE fluorcarbonates (*27*, *50*, *64*, *65*), leaving behind little evidence of the former presence of Na (*14*, *23*, *28*, *31*, *66*). Alternatively, prolonged fractionation produces enrichment of Na and REE in apatite, leaving a record of Na-rich conditions (*60*).

Carbonatites are open systems, and fenite aureoles provide evidence of Na and K transport and reaction with surrounding country rocks. This leads to a second mode of REE deposit formation, in which the structural traps are external to the carbonatites (*10*). A portion of the REE is transported as dissolved components of a carbonatite-evolved magmatic-hydrothermal fluid to the wall rocks, forming peripheral fenites.

Fenites and alkali character of natural carbonatites

Alkali feldspar-rich fenites and breccias are common in complexes that host REE-rich carbonatites. Some precipitate as LREE micromineral assemblages (less LREE-rich than the main carbonatite minerals), useful as exploration indicators (*10*, *22*) and HREE minerals are found peripheral to carbonatite complexes, up to kilometers from the main intrusions (*32*, *35*, *48*, *49*, *67*). Formation of these HREE assemblages by chloride ligand transport is problematic because LREEs are preferentially transported by chloride (*41*), implying that HREE assemblages should be accompanied by a hypothetical distal or later LREE phase, but these are not observed. Using our experimental results, the precipitation of LREE in burbankite and HREE transport by fluids into the fenite aureole in the country rock, as predicted by run CbNa, would fit this observation. If formed, then HREE-enriched natroburbankite would rapidly destabilize and release additional HREE. The increased solubility of HREE over LREE in run CbK also further enhances transport of HREE. The near wt %–level solubility of REE overwhelms in alkaline systems any minor contribution of simple REE–anion complexes such as chlorides (*40*, *46*). Furthermore, Na facilitates solubility of P and F, evident by the phosphates moraskoite and bonshtedtite observed in run CbNa, solving the apparent paradox of fluorapatite mobility in nonacidic fluids (*41*, *43*, *44*).

Carbonatites preserved in the geological record are mostly calcic, containing no alkali phases other than silicates. Fluid and melt inclusions in carbonatites or fenites are often highly alkali-rich (*11*, *13*–*16*, *34*, *36*, *49*, *50*, *62*, *68*–*70*), suggesting original liquid compositions equivalent to the combined composition of both carbonatites and fenites. Our experiments support this duality: An originally homogenous alkali-bearing carbonatite crystallized to an assemblage of solid calcic carbonates with a separate alkali-rich fluid, which in nature fenitizes the surrounding rock (*10*, *14*, *66*). Curiously, the discussion around fluid inclusions often states the high alkali contents but overlooks the role of alkali-complexing for REE mobility and instead focuses on individual anions as the drivers of REE mobility (*10*, *15*).

Fenites often have lower LREE/HREE ratios (i.e., higher HREE proportions), than their associated carbonatites (*10*, *21*, *22*, *24*). Given our experimental results, we interpret these field observations as follows. Alkali fluids exsolved from crystallizing carbonatite mobilize REE—of higher HREE/LREE ratio than is left behind in the carbonatite—to the surrounding rocks. Whereas alkali-carbonate fluids are in equilibrium with the carbonatite, they are not in equilibrium with silicate rocks. The fluids alter the siliceous prefenitized wallrocks by formation of fenite minerals such as albite, aegirine, biotite, or orthoclase, losing the Na or K required for REE mobilization. The REE then precipitate as alkali-free phases with other coexisting anions in the fluid (e.g., phosphate or carbonate), forming the same relatively insoluble phases that would have formed in the carbonatite itself had there not been alkalis to mobilize the REE (*48*, *67*, *71*).

Si inhibits REE mobility

Our experiments show that in general, Si causes sequestration of REE in apatite inside a carbonatite, whereas alkalis allow REE to concentrate elsewhere in the carbonatite or migrate outward until they eventually precipitate as REE fluorcarbonates or monazite. Natural carbonatites are expected to contain both alkalis and Si, and questions remain regarding their combined effect. Silica and alkalis would form alkali-rich silicates such as aegirine, arfvedsonite, alkali feldspars, and phlogopite. The occurrence of this reaction is demonstrated by fenites trapped as fluid inclusions at Kalkfeld, Namibia (*14*). The solubility of Si in carbonatites is usually low, particularly at upper crustal conditions (*72*). Thus, potentially ore-bearing carbonatites are expected to obtain Si primarily by wallrock contamination (*20*, *61*, *73*, *74*), putting an emphasis on the overall geological setting of a carbonatite as a controlling factor in REE ore distribution. For example, the Miaoya complex, China, hosts a carbonatite immiscible with a K-rich syenite; thus, the carbonatite should have contained the alkalis required to form a REE-bearing fenite adjacent to the carbonatite intrusion, yet no fenites are observed (*75*). The Miaoya carbonatites contain abundant allanite and biotite, indicating Si and Al contribution from the surrounding metamorphic rocks, which probably served to sequester the alkalis within

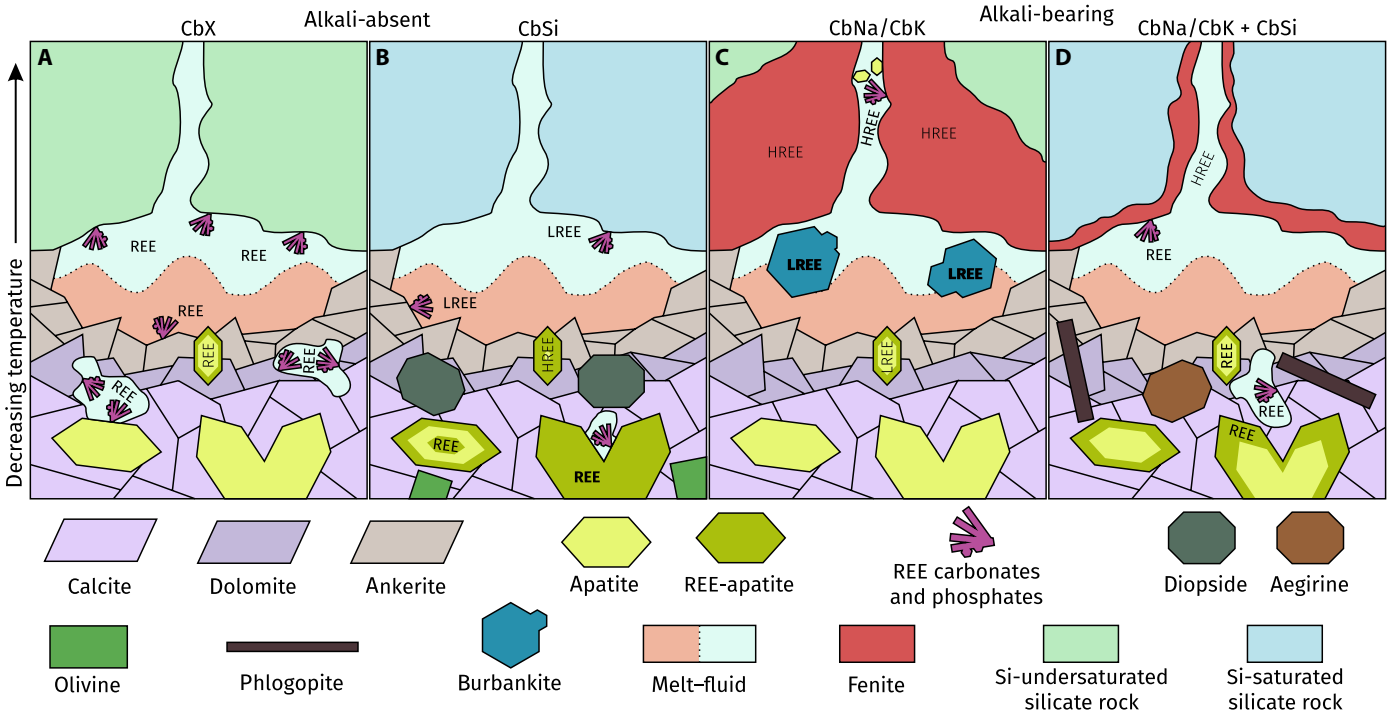

Fig. 4. Schematic representation of four potential scenarios based on our experimental results. "L/HREE" annotation denotes higher or lower LREE/HREE ratios, with letter thickness proportional to concentration. Dotted line separating melt and fluid fields represents a continuous, ill-defined transition. (**A**) Alkali-free carbonatite intruding silica-undersaturated rocks (i.e., nepheline or other feldspathoids) produces minor REE-enrichment in late apatite. Most REE hosted in carbonates and phosphates (e.g., bastnäsite, ancylite, and monazite) distributed homogenously throughout the low-temperature zone of the carbonatite. If volumetrically limited, then REE contents may be of economic grade. (**B**) Alkali-free carbonatite intruding silica-saturated rocks (i.e., feldspars ± quartz) loses most REE into early crystallizing apatite. Late-stage apatite may be HREE enriched, and minor LREE mineralization is expected to occur in late-stage REE carbonates and phosphates. The economic potential of the deposit will be upgraded if late-stage alteration redistributes REE into carbonates. This scenario is analogous to Nolans-type deposits. (**C**) Alkali-rich carbonatite intruding silica-undersaturated rocks with most of its LREE concentrated into alkali REE carbonates such as burbankites and some HREE migrating into an extensive peripheral fenite alteration zone. Burbankite is unlikely to survive alteration (by fluids varying from deuteric to weathering) although its former presence is established by REE-rich pseudomorphs. This scenario is analogous to deposits hosted in ferrous dolomite carbonatites and associated fenites (e.g., Malawi type). (**D**) Alkali-rich carbonatite intruding silica-saturated rocks, with most of its alkalis found within silicates (e.g., aegirine and phlogopite). The resultant fenite is spatially limited with no extensive REE, and most REE are found within the carbonatite body, similar to (A). This scenario is analogous to deposits found in the Mianning-Dechang belt, China.

the carbonatites and thus limit REE mobility. Similarly, mineralization at Maoniuping, China, is hosted within a granite-hosted carbonatite that contains aegirine, arvedsonite, biotite, and alkali feldspars (*53*). The surrounding fenite is volumetrically negligible and contains little REE mineralization (*50*, *63*, *70*). Elsewhere in China, HREE-rich carbonatites are also characterized by abundant silicate minerals such as aegirine and K feldspar formed by Si assimilation from the country rock (*51*, *76*), again limiting HREE loss by sequestering alkalis, resulting in HREE mineralization within the carbonatite. In contrast, silicate-poor carbonatites may lose a portion of their REE to the surrounding fenites (*22*, *49*, *65*, *67*). For example, potassic fenites adjacent to the Bear Lodge carbonatite in Wyoming are more HREE enriched than the carbonatite, whereas the carbonatite itself has a higher LREE/HREE ratio and preferentially retained the LREE (*48*). HREE transport produced xenotime in carbonatite (*59*) and also in albite-rich fenite at "Area 4," Lofdal, Namibia, and this was likely promoted by alkalis (*77*). We expect this effect to be strongest in systems hosted by silica-undersaturated rocks.

Conclusions

We find that REE are incompatible during all igneous differentiation stages in carbonatites. In alkali-free carbonatites, REEs concentrate via short-distance fluid transport in potentially economic domains within the carbonatites, where they are hosted by the relatively insoluble REE carbonates and phosphates (Fig. 4, A and B). Alkali-bearing carbonatites are capable of exsolving REE-rich fluids that can migrate long distances while retaining high REE solubilities (Fig. 4C). Both Na and K produce higher HREE/LREE ratios in the transported fluids, but potassic fluids preferentially transport HREE relative to sodic fluids. Therefore, while both LREE and HREE are expected in sodic fenites, we expect potassic fenites to contain the highest HREE/LREE ratios, consistent with observations from nature (*22*, *48*, *56*). Carbonatites intruding siliceous rocks can assimilate SiO_2, which negates this ore-forming potential by partitioning some (but not all) REEs into early-crystallizing apatite [e.g., at Nolans Bore, Australia (*78*)] and by loss of alkalis into early-crystallizing silicate minerals (*73*). Therefore, REE mineralization is confined to the carbonatite body itself (*54*), and valuable REEs such as Nd and Dy are diluted with the LREE La and Ce. Fenites around these Si-bearing carbonatites are expected to be small and barren (Fig. 4D).

Our study explains the formation of LREE-dominated deposits in carbonatites. In addition, some potential HREE carbonatite–associated deposits are expected to be hosted in potassic fenites formed around silica poor carbonatites. Alternatively, HREE deposits within carbonatites are expected to be hosted in either silica-rich and/or alkali-poor systems. Even when fenite-hosted HREE deposits are not economic, they can indicate that their host carbonatite had experienced LREE concentration by alkali-fluid migration, with potential deposition in burbankite-rich zones. Thus, the higher HREE/LREE signature of fenites is a potential exploration indicator that can help vector toward a mineralized carbonatite (*10*, *13*, *22*).

Our results are applicable to not only carbonatites sensu stricto but also other REE-rich and HREE-enriched occurrences hosted in carbonatite-absent alkaline systems, in which postmagmatic fluids are commonly rich in alkalis, carbonate, and halogens (*52*, *53*, *71*).

MATERIALS AND METHODS

Starting materials for piston cylinder experiments were prepared by mixing the reagents listed in Table 1 in an agate mortar and pestle with acetone. Composition CbX was prepared first and was then used to prepare the three other mixes (CbSi, CbNa, and CbK). About 5 mg of graphite and 200 mg of each starting mix were added to high-volume cold-weld–type capsules prefabricated from silver or nickel, and at least 10 mg of 1 M $CaBr_2$ solution was pipetted to the capsule before swaging a lid on top.

Experimental runs were performed in an end-loaded piston cylinder apparatus at the Research School of Earth Sciences, Australian National University. The initial high pressure of run CbX (2.5 GPa) was necessitated by the use of Ag capsule material, as it will melt at lower pressures. Subsequent runs consisted of higher melting point Ni capsules that permitted the higher temperature segments of the experiments to begin at 1.5 GPa. Run CbX consisted of a 5/8″ assembly with NaCl and MgO pressure mediums, whereas the later runs consisted of a 3/4″ assembly with talc and MgO pressure mediums. A thin graphite foil was used as the heater for all runs. Pressure and temperature were controlled using an automated in-house control system that allows continuous and smooth variations in pressure and temperature. Decompression was conducted using a computer-controlled valve. Quenching to room temperature took around 10 s and was done by shutting off the power supply to the heater.

After each experimental run, the capsule was removed from the assembly and mounted in epoxy resin. After hardening, a mechanical diamond lap was used to grind down the thick capsule walls to just expose a small hole from which vapor bubbles emerged. The capsule was immediately wiped and dried for about 1 hour in a 110°C oven, sanded using 180-grit sandpaper to widen the hole, and filled with epoxy resin again. After hardening, each capsule was sectioned in two halves using kerosene as a lubricant to avoid loss of water-soluble phases, and the two halves were again mounted in epoxy resin. Final polishing was conducted using 1200-, 2000-, and 4000-grit sandpaper, followed by 3-, 1-, and 0.25-μm diamond paste. The samples were cleaned between polishing steps using hexane and petroleum benzine.

Mineral maps were obtained using an FEI Quanta QEMSCAN field-emission scanning electron microscopy equipped with two Bruker 30-mm^2 EDS detectors. Acquisition conditions were 15-kV accelerating voltage, 10-nA beam current, and 10-μm step size. Image stitching was done using iDiscover and energy-dispersive spectroscopy (EDS) spectrum fitting using NanoMin.

MIR (mid-infrared region) spectra were collected for mineral phases with low electron probe microanalysis (EPMA) analytical totals, to test for H_2O, OH^-, or carbonate. ATR (attenuated total reflectance) measurements were performed using a Ge crystal objective, mounted on a Bruker A590 infrared microscope, and connected to a Bruker IFS28 spectrometer and a liquid nitrogen–cooled mercury cadmium telluride detector. The Ge crystal tip is circular, with 100-μm diameter. Background and sample measurements were performed on a 37.5 μm by 37.5 μm area and consisted of 180 scans, with a spectral resolution of 2 cm^{-1} in the 600- to 4000-cm^{-1} range. The Ge crystal surface was pressed on the sample with a 4-N force for enhancing contact. The resulting spectra underwent atmospheric correction, interactive concave rubber band baseline correction, and extended ATR correction using the OPUS software. ATR correction accounted for the shift and drop in absorption

band intensity caused by the penetration depth of the evanescent wave into the sample and its dispersion.

Quantitative wavelength-dispersive spectroscopy (WDS) analyses were conducted using a JEOL 8530F Plus Electron Probe Microanalyzer (EPMA). Full WDS spectrometer scans were obtained on key phases to identify elements and determine peak and background positions. Acquisition conditions were 15-kV accelerating voltage and 10-nA beam current. Beam diameter was 2 μm for fluorapatite and bastnäsite and 15 μm for all other phases. The following Astimex reference materials were used: diopside (Si-Kα, Ca-Kα, and Mg-Kα), thallium bromide iodide (Br-Lα), fluorapatite (P-Kα), albite (Na-Kα), lanthanum pentaphosphate (La-Lα), sanidine (K-Kα), hematite (Fe-Kα), fluorite (F-Kα), dysprosium pentaphosphate (Dy-Lα), pentlandite (Ni-Kα), and tugtupite (Cl-Kα). Analyzing crystals were TAP (F, Si, Mg, Br, and Na), PET (Cl, Ca, P, and K), and LIF (Dy, La, Fe, and Ni). Volatile elements (Na, K, Cl, Br, and F) were analyzed first. Even with the defocused beam, Na counts would strongly decrease within seconds, whereas counts for other elements would increase due to the lack of absorbing Na. Therefore, for Na-rich minerals, reported Na contents are a minimum, whereas other elements (commonly Ca, Mg, La, Dy, and Fe) are a maximum. Likewise, F and Br would readily volatilize, but to a lesser degree than Na. We estimate the reported numbers to be correct to within 10% of the real value. Fluorine counts are known to increase in fluorapatite when using a beam diameter of 2 μm. As we were mostly interested in La and Dy contents of fluorapatite, no attempt was made to accurately measure F. Reported values should be considered as maximum values.

SUPPLEMENTARY MATERIALS

Supplementary material for this article is available at http://advances.sciencemag.org/cgi/content/full/6/41/eabb6570/DC1

REFERENCES AND NOTES

1. B. K. Sovacool, S. H. Ali, M. Bazilian, B. Radley, B. Nemery, J. Okatz, D. Mulvaney, Sustainable minerals and metals for a low-carbon future. *Science* **367**, 30–33 (2020).
2. Z. Weng, S. M. Jowitt, G. M. Mudd, N. Haque, A detailed assessment of global rare earth element eesources: Opportunities and challenges. *Econ. Geol.* **110**, 1925–1952 (2015).
3. K. Hund, D. La Porta, T. P. Fabregas, T. Laing, J. Drexhage, *Minerals for Climate Action: The Mineral Intensity of the Clean Energy Transition* (The World Bank, 2020).
4. A. R. Chakhmouradian, F. Wall, Rare earth elements: Minerals, mines, magnets (and more). *Elements* **8**, 333–340 (2012).
5. R. L. Linnen, I. M. Samson, A. E. Williams-Jones, A. R. Chakhmouradian, in *Geochemistry of Mineral Deposits*, S. D. Scott, Ed. (Vol 13, *Treatise on Geochemistry*, Second Edition; Elsevier Science, 2014), chap. 21, pp. 543–568.
6. F. Wall, in *Critical Metals Handbook*, G. Gunn, Ed. (John Wiley & Sons, Chichester, West Sussex, United Kingdom, 2014), chap. 13, pp. 312–339.
7. K. M. Goodenough, F. Wall, D. Merriman, The rare earth elements: Demand, global resources, and challenges for resourcing future generations. *Nat. Resour. Res.* **27**, 201–216 (2018).
8. P. L. Verplanck, A. N. Mariano, A. Mariano Jr., in *Rare Earth and Critical Elements in Ore Deposits*, P. L. Verplanck, M. W. Hitzman, Eds. (Society of Economic Geologists, Littleton, Colorado, USA, 2016), chap. 1, pp. 5–32.
9. F. Wall, A. Rollat, R. S. Pell, Responsible sourcing of critical metals. *Elements* **13**, 313–318 (2017).
10. H. A. L. Elliott, F. Wall, A. R. Chakhmouradian, P. R. Siegfried, S. Dahlgren, S. Weatherley, A. A. Finch, M. A. W. Marks, E. Dowman, E. Deady, Fenites associated with carbonatite complexes: A review. *Ore Geol. Rev.* **93**, 38–59 (2018).
11. A. G. Bulakh, V. V. Ivanikov, Carbonatites of the Turiy Peninsula, Kola: Role of magmatism and of metasomatism. *Can. Mineral.* **34**, 403–409 (1996).
12. A. N. Mariano, in *Carbonatites: Genesis and Evolution*, K. Bell, Ed. (Unwin Hyman, London, 1989), chap. 7, pp. 149–176.
13. G. J. Simandl, S. Paradis, Carbonatites: Related ore deposits, resources, footprint, and exploration methods. *Appl. Earth Sci.* **127**, 123–152 (2018).
14. B. Bühn, A. H. Rankin, Composition of natural, volatile-rich Na–Ca–REE–Sr carbonatitic fluids trapped in fluid inclusions. *Geochim. Cosmochim. Acta* **63**, 3781–3797 (1999).
15. B. Bühn, A. H. Rankin, M. Radtke, M. Haller, A. Knöchel, Burbankite, a (Sr, REE, Na, Ca)-carbonate in fluid inclusions from carbonatite-derived fluids: Identification and characterization using laser Raman spectroscopy, SEM-EDX, and synchrotron micro-XRF analysis. *Am. Mineral.* **84**, 1117–1125 (1999).
16. B. F. Walter, M. Steele-MacInnis, R. J. Giebel, M. A. W. Marks, G. Markl, Complex carbonate-sulfate brines in fluid inclusions from carbonatites: Estimating compositions in the system H_2O-Na-K-CO_3-SO_4-Cl. *Geochim. Cosmochim. Acta* **277**, 224–242 (2020).
17. P. L. Verplanck, B. S. Van Gosen, R. R. Seal, A. E. McCafferty, "A deposit model for carbonatite and peralkaline intrusion-related rare earth element deposits" (U.S. Geological Survey Scientific Investigations Report 2010–5070–J, Reston, Virginia, 2014).
18. H. A. Buckley, A. R. Woolley, Carbonates of the magnesite–siderite series from four carbonatite complexes. *Mineral. Mag.* **54**, 413–418 (1990).
19. A. A. Frolov, Vertical zonation in deposition of ore, as in ultrabasic-alkaline rocks and carbonatites. *Int. Geol. Rev.* **13**, 685–695 (1971).
20. A. G. Doroshkevich, S. G. Viladkar, G. S. Ripp, M. V. Burtseva, Hydrothermal REE mineralization in the Amba Dongar carbonatite complex, Gujarat, India. *Can. Mineral.* **47**, 1105–1116 (2009).
21. J. Trofanenko, A. E. Williams-Jones, G. J. Simandl, A. A. Migdisov, The nature and origin of the REE mineralization in the Wicheeda Carbonatite, British Columbia, Canada. *Econ. Geol.* **111**, 199–223 (2016).
22. E. Dowman, F. Wall, P. J. Treloar, A. H. Rankin, Rare-earth mobility as a result of multiple phases of fluid activity in fenite around the Chilwa Island Carbonatite, Malawi. *Mineral. Mag.* **81**, 1367–1395 (2017).
23. A. Néron, L. Bédard, D. Gaboury, The Saint-Honoré carbonatite REE zone, Québec, Canada: Combined magmatic and hydrothermal processes. *Minerals* **8**, 397 (2018).
24. S. Decrée, G. Cawthorn, E. Deloule, J. Mercadier, H. Frimmel, J.-M. Baele, Unravelling the processes controlling apatite formation in the Phalaborwa Complex (South Africa) based on combined cathodoluminescence, LA-ICPMS and in-situ O and Sr isotope analyses. *Contrib. Mineral. Petrol.* **175**, 34 (2020).
25. S. Klemme, C. Dalpé, Trace-element partitioning between apatite and carbonatite melt. *Am. Mineral.* **88**, 639–646 (2003).
26. A. R. Chakhmouradian, E. P. Reguir, A. N. Zaitsev, C. Couëslan, C. Xu, J. Kynický, A. H. Mumin, P. Yang, Apatite in carbonatitic rocks: Compositional variation, zoning, element partitioning and petrogenetic significance. *Lithos* **274–275**, 188–213 (2017).
27. A. N. Zaitsev, A. R. Chakhmouradian, Calcite–amphibole–clinopyroxene rock from the Afrikanda complex, Kola Peninsula, Russia: Mineralogy and a possible link to carbonatites. II. Oxysalt minerals. *Can. Mineral.* **40**, 103–120 (2002).
28. M. Smith, J. Kynicky, C. Xu, W. Song, J. Spratt, T. Jeffries, M. Brtnicky, A. Kopriva, D. Cangelosi, The origin of secondary heavy rare earth element enrichment in carbonatites: Constraints from the evolution of the Huanglongpu district, China. *Lithos* **308–309**, 65–82 (2018).
29. E. Kozlov, E. Fomina, M. Sidorov, V. Shilovskikh, V. Bocharov, A. Chernyavsky, M. Huber, The Petyayan-Vara carbonatite-hosted rare earth deposit (Vuoriyarvi, NW Russia): Mineralogy and geochemistry. *Minerals* **10**, 73 (2020).
30. R. J. Giebel, C. D. K. Gauert, M. A. W. Marks, G. Costin, G. Markl, Multi-stage formation of REE minerals in the Palabora Carbonatite Complex, South Africa. *Am. Mineral.* **102**, 1218–1233 (2017).
31. A. N. Zaitsev, A. Demény, S. Sindern, F. Wall, Burbankite group minerals and their alteration in rare earth carbonatites—Source of elements and fluids (evidence from C–O and Sr–Nd isotopic data). *Lithos* **62**, 15–33 (2002).
32. F. Wall, A. N. Mariano, in *Rare Earth Minerals: Chemistry, Origin and Ore Deposits*, A. P. Jones, F. Wall, C. T. Williams, Eds. (Chapman & Hall, London, 1996), pp. 193–226.
33. A. K. Andersen, J. G. Clark, P. B. Larson, J. J. Donovan, REE fractionation, mineral speciation, and supergene enrichment of the Bear Lodge carbonatites, Wyoming, USA. *Ore Geol. Rev.* **89**, 780–807 (2017).
34. I. Prokopyev, E. Kozlov, E. Fomina, A. Doroshkevich, M. Dyomkin, Mineralogy and fluid regime of formation of the REE-late-stage hydrothermal mineralization of Petyayan-Vara carbonatites (Vuoriyarvi, Kola Region, NW Russia). *Minerals* **10**, 405 (2020).
35. S. Broom-Fendley, F. Wall, B. Spiro, C. V. Ullmann, Deducing the source and composition of rare earth mineralising fluids in carbonatites: Insights from isotopic (C, O, $^{87}Sr/^{86}Sr$) data from Kangankunde, Malawi. *Contrib. Mineral. Petrol.* **172**, 96 (2017).
36. V. S. Kamenetsky, R. H. Mitchell, R. Maas, A. Giuliani, D. Gaboury, L. Zhitova, Chlorine in mantle-derived carbonatite melts revealed by halite in the St.-Honoré intrusion (Québec, Canada). *Geology* **43**, 687–690 (2015).
37. A. M. McDonald, G. Y. Chao, R. A. Ramik, Rouvilleite, a new sodium calcium fluorocarbonate mineral from Mont Saint-Hilaire, Quebec. *Can. Mineral.* **29**, 107–111 (1991).
38. A. P. Khomyakov, Bonshtedtite, $Na_3Fe(PO_4)(CO_3)$ – A new mineral. *Int. Geol. Rev.* **25**, 368–372 (1983).
39. A. Migdisov, X. Guo, H. Nisbet, H. Xu, A. E. Williams-Jones, Fractionation of REE, U, and Th in natural ore-forming hydrothermal systems: Thermodynamic modeling. *J. Chem. Thermodyn.* **128**, 305–319 (2019).

40. L. Zhou, J. Mavrogenes, C. Spandler, H. Li, A synthetic fluid inclusion study of the solubility of monazite-(La) and xenotime-(Y) in H_2O-Na-K-Cl-F-CO_2 fluids at 800 °C and 0.5 GPa. *Chem. Geol.* **442**, 121–129 (2016).
41. A. Migdisov, A. E. Williams-Jones, J. Brugger, F. A. Caporuscio, Hydrothermal transport, deposition, and fractionation of the REE: Experimental data and thermodynamic calculations. *Chem. Geol.* **439**, 13–42 (2016).
42. E. A. Tanis, A. Simon, O. Tschauner, P. Chow, Y. Xiao, G. Shen, J. M. Hanchar, M. Frank, Solubility of xenotime in a 2 M HCl aqueous fluid from 1.2 to 2.6 GPa and 300 to 500 °C. *Am. Mineral.* **97**, 1708–1713 (2012).
43. M. Louvel, A. Bordage, D. Testemale, L. Zhou, J. Mavrogenes, Hydrothermal controls on the genesis of REE deposits: Insights from an *in situ* XAS study of Yb solubility and speciation in high temperature fluids (T < 400 °C). *Chem. Geol.* **417**, 228–237 (2015).
44. M. Anenburg, A. D. Burnham, J. A. Mavrogenes, REE redistribution textures in altered fluorapatite: Symplectites, veins and phosphate-silicate-carbonate assemblages from the Nolans Bore P-REE-Th deposit, NT, Australia. *Can. Mineral.* **56**, 331–354 (2018).
45. A. P. Gysi, A. E. Williams-Jones, D. Harlov, The solubility of xenotime-(Y) and other HREE phosphates ($DyPO_4$, $ErPO_4$ and $YbPO_4$) in aqueous solutions from 100 to 250 °C and p_{sat}. *Chem. Geol.* **401**, 83–95 (2015).
46. A. Tsay, Z. Zajacz, C. Sanchez-Valle, Efficient mobilization and fractionation of rare-earth elements by aqueous fluids upon slab dehydration. *Earth Planet. Sci. Lett.* **398**, 101–112 (2014).
47. M. J. Reed, P. A. Candela, P. M. Piccoli, The distribution of rare earth elements between monzogranitic melt and the aqueous volatile phase in experimental investigations at 800 °C and 200 MPa. *Contrib. Mineral. Petrol.* **140**, 251–262 (2000).
48. A. K. Andersen, J. G. Clark, P. B. Larson, O. K. Neill, Mineral chemistry and petrogenesis of a HFSE(+HREE) occurrence, peripheral to carbonatites of the Bear Lodge alkaline complex, Wyoming. *Am. Mineral.* **101**, 1604–1623 (2016).
49. S. Broom-Fendley, A. E. Brady, F. Wall, G. Gunn, W. Dawes, REE minerals at the Songwe Hill carbonatite, Malawi: HREE-enrichment in late-stage apatite. *Ore Geol. Rev.* **81**, 23–41 (2017).
50. X. Zheng, Y. Liu, Mechanisms of element precipitation in carbonatite-related rare-earth element deposits: Evidence from fluid inclusions in the Maoniuping deposit, Sichuan Province, southwestern China. *Ore Geol. Rev.* **107**, 218–238 (2019).
51. D. Cangelosi, M. Smith, D. Banks, B. Yardley, The role of sulfate-rich fluids in heavy rare earth enrichment at the Dashigou carbonatite deposit, Huanglongpu, China. *Mineral. Mag.* **84**, 65–80 (2020).
52. A. A. Arzamastsev, L. V. Arzamastseva, G. P. Zaraiskii, Contact interaction of agpaitic magmas with basement gneisses: An example of the Khibina and Lovozero Massifs. *Petrology* **19**, 109–133 (2011).
53. Y. Liu, A. R. Chakhmouradian, Z. Hou, W. Song, J. Kynický, Development of REE mineralization in the giant Maoniuping deposit (Sichuan, China): Insights from mineralogy, fluid inclusions, and trace-element geochemistry. *Miner. Deposita* **54**, 701–718 (2019).
54. Y.-C. Ying, W. Chen, A. Simonetti, S.-Y. Jiang, K.-D. Zhao, Significance of hydrothermal reworking for REE mineralization associated with carbonatite: Constraints from in situ trace element and C-Sr isotope study of calcite and apatite from the Miaoya carbonatite complex (China). *Geochim. Cosmochim. Acta* **280**, 340–359 (2020).
55. S. Broom-Fendley, A. E. Brady, M. S. A. Horstwood, A. R. Woolley, J. Mtegha, F. Wall, W. Dawes, G. Gunn, Geology, geochemistry and geochronology of the Songwe Hill carbonatite, Malawi. *J. Afr. Earth Sci.* **134**, 10–23 (2017).
56. S. Decrée, P. Boulvais, C. Cobert, J.-M. Baele, G. Midende, V. Gardien, L. Tack, G. Nimpagaritse, D. Demaiffe, Structurally-controlled hydrothermal alteration in the syntectonic Neoproterozoic Upper Ruvubu Alkaline Plutonic Complex (Burundi): Implications for REE and HFSE mobilities. *Precambrian Res.* **269**, 281–295 (2015).
57. T. Andersen, Compositional variation of some rare earth minerals from the Fen complex (Telemark, SE Norway): Implications for the mobility of rare earths in a carbonatite system. *Mineral. Mag.* **50**, 503–509 (1986).
58. C. Marien, A. H. Dijkstra, C. Wilkins, The hydrothermal alteration of carbonatite in the Fen Complex, Norway: Mineralogy, geochemistry, and implications for rare-earth element resource formation. *Mineral. Mag.* **82**, S115–S131 (2018).
59. F. Wall, V. N. Niku-Paavola, C. Storey, A. Muller, T. Jeffries, Xenotime-(Y) from carbonatite dykes at Lofdal, Namibia: Unusually low LREE:HREE ratio in carbonatite, and the first dating of xenotime overgrowths on zircon. *Can. Mineral.* **46**, 861–877 (2008).
60. A.-V. Walter, R. Flicoteaux, C. Parron, M. Loubet, D. Nahon, Rare-earth elements and isotopes (Sr, Nd, O, C) in minerals from the Juquiá carbonatite (Brazil): Tracers of a multistage evolution. *Chem. Geol.* **120**, 27–44 (1995).
61. W. T. Pecora, in *Petrologic Studies,* A. E. J. Engel, H. L. James, B. F. Leonard, Eds. (Geological Society of America, 1962), chap. 4, pp. 83–104.
62. X. Shu, Y. Liu, D. Li, Fluid inclusions as an indicator for REE mineralization in the Lizhuang deposit, Sichuan Province, Southwest China. *J. Geochem. Explor.* **213**, 106518 (2020).
63. J. Yuheng, L. Yan, Factors controlling the generation and diversity of giant carbonatite-related rare earth element deposits: Insights from the Mianning–Dechang belt. *Ore Geol. Rev.* **121**, 103472 (2020).
64. M. Moore, A. R. Chakhmouradian, A. N. Mariano, R. Sidhu, Evolution of rare-earth mineralization in the Bear Lodge carbonatite, Wyoming: Mineralogical and isotopic evidence. *Ore Geol. Rev.* **64**, 499–521 (2015).
65. C. A. F. Dietzel, T. Kristandt, S. Dahlgren, R. J. Giebel, M. A. W. Marks, T. Wenzel, G. Markl, Hydrothermal processes in the Fen alkaline-carbonatite complex, southern Norway. *Ore Geol. Rev.* **111**, 102969 (2019).
66. I. V. Veksler, H. Keppler, Partitioning of Mg, Ca, and Na between carbonatite melt and hydrous fluid at 0.1–0.2 GPa. *Contrib. Mineral. Petrol.* **138**, 27–34 (2000).
67. S. Broom-Fendley, M. T. Styles, J. D. Appleton, G. Gunn, F. Wall, Evidence for dissolution-reprecipitation of apatite and preferential LREE mobility in carbonatite-derived late-stage hydrothermal processes. *Am. Mineral.* **101**, 596–611 (2016).
68. T. Guzmics, Z. Zajacz, R. H. Mitchell, C. Szabó, M. Wälle, The role of liquid–liquid immiscibility and crystal fractionation in the genesis of carbonatite magmas: Insights from Kerimasi melt inclusions. *Contrib. Mineral. Petrol.* **169**, 17 (2015).
69. T. Guzmics, R. H. Mitchell, C. Szabó, M. Berkesi, R. Milke, R. Abart, Carbonatite melt inclusions in coexisting magnetite, apatite and monticellite in Kerimasi calciocarbonatite, Tanzania: Melt evolution and petrogenesis. *Contrib. Mineral. Petrol.* **161**, 177–196 (2011).
70. Y. Xie, Y. Li, Z. Hou, D. R. Cooke, L. Danyushevsky, S. C. Dominy, S. Yin, A model for carbonatite hosted REE mineralisation — the Mianning–Dechang REE belt, Western Sichuan Province, China. *Ore Geol. Rev.* **70**, 595–612 (2015).
71. V. C. Honour, K. M. Goodenough, R. A. Shaw, I. Gabudianu, P. Hirtopanu, REE mineralisation within the Ditrău Alkaline Complex, Romania: Interplay of magmatic and hydrothermal processes. *Lithos* **314-315**, 360–381 (2018).
72. M. Massuyeau, E. Gardés, Y. Morizet, F. Gaillard, A model for the activity of silica along the carbonatite–kimberlite–mellilitite–basanite melt compositional joint. *Chem. Geol.* **418**, 206–216 (2015).
73. R. J. Giebel, A. Parsapoor, B. F. Walter, S. Braunger, M. A. W. Marks, T. Wenzel, G. Markl, Evidence for magma–wall rock interaction in carbonatites from the Kaiserstuhl Volcanic Complex (Southwest Germany). *J. Petrol.* **60**, 1163–1194 (2019).
74. M. Anenburg, J. A. Mavrogenes, Carbonatitic versus hydrothermal origin for fluorapatite REE-Th deposits: Experimental study of REE transport and crustal "antiskarn" metasomatism. *Am. J. Sci.* **318**, 335–366 (2018).
75. J.-H. Su, X.-F. Zhao, X.-C. Li, W. Hu, M. Chen, Y.-L. Xiong, Geological and geochemical characteristics of the Miaoya syenite-carbonatite complex, Central China: Implications for the origin of REE-Nb-enriched carbonatite. *Ore Geol. Rev.* **113**, 103101 (2019).
76. T. Bai, W. Chen, S.-Y. Jiang, Evolution of the carbonatite Mo-HREE deposits in the Lesser Qinling Orogen: Insights from in situ geochemical investigation of calcite and sulfate. *Ore Geol. Rev.* **113**, 103069 (2019).
77. D. Dodd, P. Hannon, W. Roy, P. Siegfried, M. Hall, Preliminary economic assessment on the Lofdal rare earths project, Namibia: 1393S1-NI-43-101 (Namibia Rare Earths Inc., SEDAR, 2014).
78. M. Anenburg, J. A. Mavrogenes, V. C. Bennett, The fluorapatite P-REE-Th vein deposit at Nolans Bore: Genesis by carbonatite metasomatism. *J. Petrol.* **61**, egaa003 (2020).

Acknowledgments: We thank Z. Zajacz for insightful reviews. We acknowledge the facilities and assistance of F. Brink, H. Chen, and J. Chen at the Centre for Advanced Microscopy, Australian National University. **Funding:** This research was funded by NERC SoS RARE consortium, grant number NE/M011429/1. **Author contributions:** M.A. prepared and performed the experiments and performed EPMA and QEMSCAN analyses. C.F. performed FTIR analyses. All authors contributed to discussions and the paper. **Competing interests:** The authors declare that they have no competing interests. **Data and materials availability:** All data needed to evaluate the conclusions in the paper are present in the paper and the Supplementary Materials. Additional data related to this paper may be requested from the authors.

Submitted 9 March 2020
Accepted 17 August 2020
Published 9 October 2020
10.1126/sciadv.abb6570

Citation: M. Anenburg, J. A. Mavrogenes, C. Frigo, F. Wall, Rare earth element mobility in and around carbonatites controlled by sodium, potassium, and silica. *Sci. Adv.* **6**, eabb6570 (2020).

ScienceAdvances

Rare earth element mobility in and around carbonatites controlled by sodium, potassium, and silica

Michael Anenburg, John A. Mavrogenes, Corinne Frigo and Frances Wall

Sci Adv **6** (41), eabb6570.
DOI: 10.1126/sciadv.abb6570